

# Aliquoting on the centrifugal microfluidic platform based on centrifugo-pneumatic valves

Daniel Mark · Patrick Weber · Sascha Lutz · Maximilian Focke · Roland Zengerle · Felix von Stetten

Received: 27 October 2010 / Accepted: 15 December 2010 / Published online: 8 January 2011  
© Springer-Verlag 2011

**Abstract** We present a new method for aliquoting liquids on the centrifugal microfluidic platform. Aliquoting is an essential unit operation to perform multiple parallel assays (“geometric multiplexing”) from one individual sample, such as genotyping by real-time polymerase chain reactions (PCR), or homogeneous immunoassay panels. Our method is a two-stage process with an initial metering phase and a subsequent transport phase initiated by switching a centrifugo-pneumatic valve. The method enables aliquoting liquids into completely separated reaction cavities. It includes precise metering that is independent on the volume of pre-stored reagents in the receiving cavities. It further excludes any cross-contamination between the receiving cavities. We characterized the performance for prototypes fabricated by three different technologies: micro-milling, thermoforming of foils, and injection molding. An initial volume of  $\sim 90 \mu\text{l}$  was split into 8 aliquots of  $10 \mu\text{l}$  volume each plus a waste reservoir on a thermoformed foil disk resulting in a coefficient of variation (CV) of the metered volumes of 3.6%. A similar volume of  $\sim 105 \mu\text{l}$  was split into 16 aliquots of  $6 \mu\text{l}$  volume each on micro-milled and injection-molded disks and the corresponding CVs were 2.8 and 2.2%, respectively.

Thus, the compatibility of the novel aliquoting structure to the aforementioned prototyping and production technologies is demonstrated. Additionally, the important question of achievable volume precision of the aliquoting structure with respect to the production tolerances inherent to each of these production technologies is addressed experimentally and theoretically. The new method is amenable to low cost mass production, since it does not require any post-replication surface modifications like hydrophobic patches.

**Keywords** Lab-on-a-chip · Centrifugal microfluidics · Aliquoting · Multiplexing · PCR · Pneumatic

## 1 Introduction

Aliquoting of liquids is an essential unit operation in the attractive application field of multi-parameter testing on centrifugal microfluidic lab-on-a-chip platforms (Haeberle and Zengerle 2007; Mark et al. 2010; Ducree et al. 2007; Madou et al. 2006; Nolte 2009; Gorkin et al. 2010). It permits splitting a liquid volume into several sub-volumes which can then be subjected to different processing and analytical reactions. Such aliquoting structures should offer precise liquid metering that is independent of any pre-stored reagents in the receiving cavities, and prevent cross-contamination between neighboring chambers.

Application fields can be clinical chemistry (Cho et al. 2008; Schembri et al. 1992) but also emerging applications, such as microfluidically integrated genotyping (Focke et al. 2010), homogeneous immunoassays (Rubenstein et al. 1972), or the detection of pathogens (Liu et al. 2004; Siegrist et al. 2010). Current microfluidic structures for liquid aliquoting are either one-stage or two-stage processes (Fig. 1).

D. Mark (✉) · S. Lutz · R. Zengerle · F. von Stetten  
HSG-IMIT, Wilhelm-Schickard-Straße 10, 78052  
Villingen-Schwenningen, Germany  
e-mail: daniel.mark@hsg-imit.de

P. Weber · M. Focke · R. Zengerle · F. von Stetten  
Laboratory for MEMS Applications, Department of  
Microsystems Engineering (IMTEK), University of Freiburg,  
Georges-Koehler-Allee 106, 79110 Freiburg, Germany

R. Zengerle  
Centre for Biological Signalling Studies—BIOSS,  
University of Freiburg, Freiburg, Germany

In one-stage aliquoting, the liquid volume is metered directly in the final reaction chambers. Such structures have the advantage of being easily designed and produced, but the disadvantage that pre-stored reagents in the reaction chamber influence the metered volume. Additionally, dissolved reagents could potentially be transported between reaction chambers during the metering process, since the liquid volume fluidically connects all reaction chambers during the complete aliquoting process (Fig. 1b). This could lead to cross-contaminations between reactions. Varying structures for one-stage aliquoting have been published for clinical chemistry applications (Schembri et al. 1992, 1995), enzymatic assays (Burtis et al. 1972), and digital PCR (Sundberg et al. 2010).

In two-stage aliquoting, liquid is first metered and split into sub-volumes at a low centrifugation frequency and then forwarded into the final reaction chambers at a high centrifugation frequency (Fig. 1c–e). Significant advantages of this approach include independent metering which is not influenced by pre-stored reagents in the receiving cavities, prevention of cross-contamination by fluidic separation of the metered volumes before they are forwarded into the receiving chambers, and simultaneous start of the assays in all reaction chambers. According to the current state-of-the-art, two-stage aliquoting relies on the use of hydrophobic valves between the metering chamber and the reaction chamber. The disadvantage of this solution is the large number of hydrophobic valves that are required. Since hydrophobic valves are local surface modifications which have to be applied with high spatial precision and exact volume, they represent a complex manufacturing step leading to increased

fabrication costs. Structures for two-stage aliquoting based on hydrophobic patches have been presented for immunoassays (Honda et al. 2005; Andersson and Ekstrand 2007) and matrix-assisted laser desorption/ionization (MALDI) sample preparation (referenced in Madou et al. 2006).

The presented state-of-the-art solutions either lack means of controlling the influence of pre-stored reagents on the metered volume and to prevent cross-contamination (one-stage aliquoting), or require a large number of microfluidic valves based on local surface modifications (two-stage aliquoting). In this study, we utilize a previously published centrifugo-pneumatic valve (Mark et al. 2009) to design a novel two-stage aliquoting method which does not need any coating or special surface treatment. This aliquoting structure features precise volume metering independent of pre-stored reagents, reduced risk of cross-contamination by complete liquid separation, simultaneous forwarding of liquid aliquots into the final receiving chambers, and requires no post-replication surface modifications. The aliquoting structure is tested with respect to the main concerns for widespread applicability: the achievable volume precision, and the compatibility to mass production technologies. Therefore, the feasibility of the novel aliquoting structure for inexpensive and easy production is demonstrated by characterizing its aliquoting precision for different prototyping and production technologies: micro-milling, thermoforming of foils, and injection molding. Thus, it is shown that this structure unites the advantages of a two-stage aliquoting process with the cheap manufacturability of a one-stage aliquoting structure.

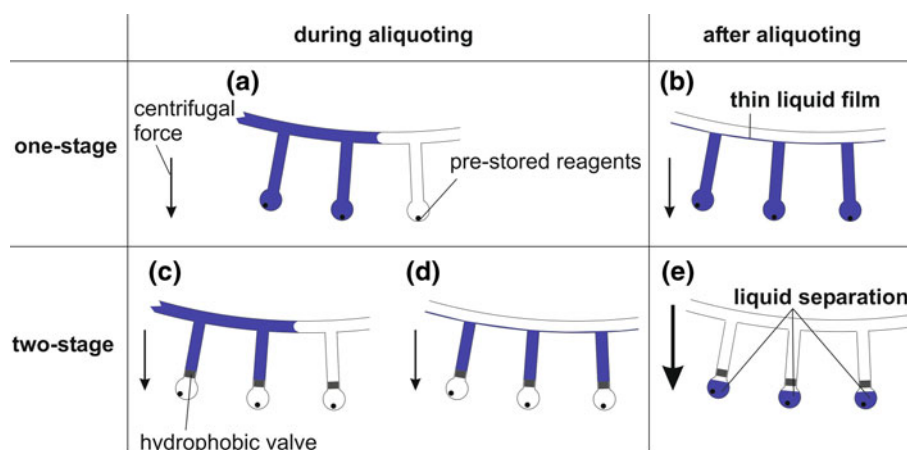


**Fig. 1** Two different state-of-the-art aliquoting principles for centrifugal microfluidic platforms. **a–b** One-stage aliquoting. During the metering process, the whole liquid volume is connected and pre-stored reagents influence the metered volume. **c** Two-stage aliquoting. During the metering phase at low centrifugal force, the liquid is not in

contact with pre-stored reagents and **d** is separated into sub-volumes before it is **e** forwarded into the reaction chambers at high centrifugal force. Two-stage aliquoting in the state-of-the-art usually requires a large number of hydrophobic valves

## 2 Materials and methods

### 2.1 Working principle

The basic principle of the aliquoting process is depicted in Fig. 2. In the first phase, liquid is introduced into the aliquoting structure via a radially slightly sloping feed channel. The liquid then enters a series of branching metering channels (Fig. 2c) and overflows into a waste chamber which results in separated sub-volumes. In the second phase, the sub-volumes are forwarded through the valve into separate receiving chambers (Fig. 2d). Cross-contamination between analytical reactions performed in neighboring receiving chambers can easily be excluded. To enable fast optical read-out of analytical reactions at a constant radial position, the slope of the feed channel has to be compensated: this is achieved by a decrease in length of the metering channels along the feed channel. To achieve uniform volumes in all metering channel, this decrease in length is compensated by a lateral widening.

The coating free centrifugo-pneumatic valve has previously been described in detail and was characterized for water, detergent concentrations between 0.01 and 10%, and pure ethanol (Mark et al. 2009). In brief, the centrifugo-pneumatic valve utilizes the phenomenon that an air-filled, unvented receiving chamber stops liquid flow until the air–liquid interface becomes unstable at high gravitational (or centrifugal) forces (Rayleigh–Taylor instability, Sharp 1984). The centrifugo-pneumatic valve has been tested over the working range of receiving chambers between 1 and 36  $\mu\text{l}$ . An extrapolation to smaller receiving chamber volumes and channels can be done with a semi-empirical equation published previously (Mark et al. 2009). Receiving chamber volumes in the nanoliter-range are feasible but predicted to require centrifugal pressures  $>100$  kPa, although the validity of the semi-empirical equation in this regime is untested. The presented working range 1–36  $\mu\text{l}$  spans the typical volumes for the microfluidic integration and automation of labor-intensive laboratory protocols, e.g. geometrically multiplexed PCR (aliquoting of a sample into individual PCR reactions for testing of several parameters in parallel).

In summary, the novel design represents an easily manufactured two-stage aliquoting structure that does not require any local surface modifications. Dry reagents can be pre-stored in the receiving chamber without changing the volume of the metering structure and thus the metered liquid sub-volumes. Analytical reactions in the receiving chambers can be performed without any cross-contaminations (Lutz et al. 2009; Focke et al. 2010).

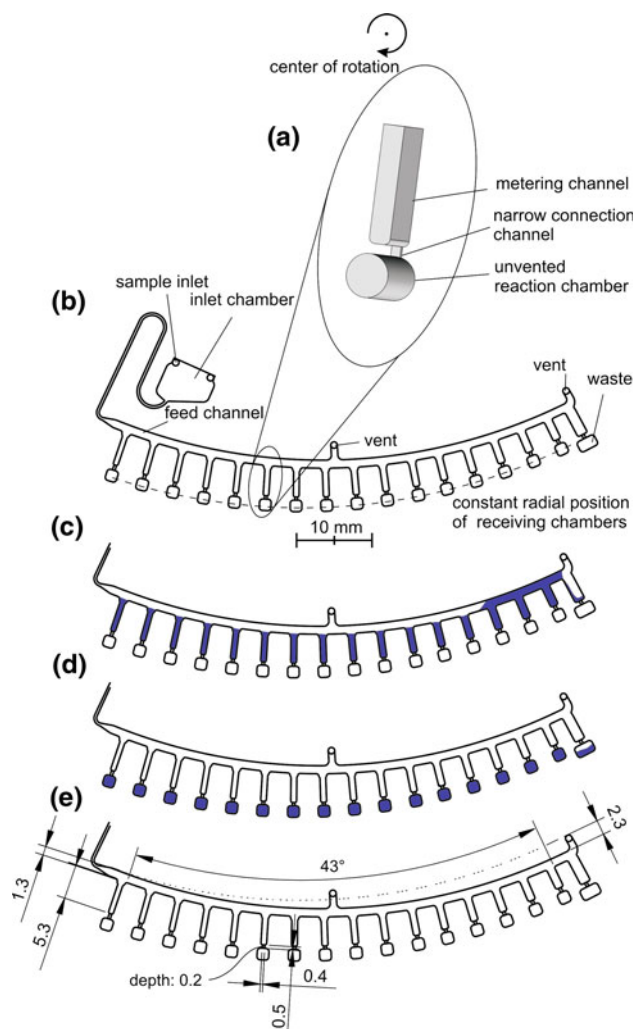


**Fig. 2** Layout and functional principle of the centrifugo-pneumatic valve and the aliquoting structure. **a** The 3D image shows a view on a single metering structure. **b** A radially inclined feed channel supports several branching metering structures. **c** Sketch of the filling process: the liquid fills the feed channel and metering structures while excess liquid overflows into the waste chamber. The unvented reaction chambers remain dry until the rotational frequency is raised above a critical value **d** which leads to filling of the reaction chambers thus separating the aliquots. **e** Relevant design parameters include: the slope of the feed channel (in this case 2.3 mm), the width and depth of the feed channel, the volume of the metering channels and receiving chamber (in this case 6  $\mu\text{l}$  for both), and the length, width, and depth of the narrow connection channel which defines the burst frequency of the centrifugo-pneumatic valve

### 2.2 Fabrication

The aliquoting structure was implemented in a thermoformed foil with a micro thermoforming by soft lithography ( $\mu\text{TSL}$ ) process described previously (Focke et al. 2010). In brief, a master structure is micro-milled in PMMA and cast in PDMS. This negative PDMS

stamp is replicated into positive-microstructured foils by thermoforming in a 188  $\mu\text{m}$  cyclic olefin polymer foil (COP, ZF14, Zeon Chemicals). Injection molding of a similar design was done by microfluidic ChipShop GmbH, Germany. Injection-molded cartridges and thermoformed foil were neither coated globally nor locally. Additionally, the aliquoting structure was micro-milled with a Minimill 3 (Minitech Machinery Corp., GA, USA) in a 4 mm cyclo-olefin-polymer (COP) disk (material from microfluidic ChipShop GmbH, Germany) using end mills with 0.4 and 1 mm diameter (F126.0040 and F113.0100, Gienger Industrie-Service, Switzerland). To render the channels of the milled disk hydrophilic, they were globally coated with poly-ethylene-glycol (PEG, molecular weight 15–20 kD, Sigma-Aldrich Chemie GmbH, Germany, concentration 5 mg PEG/ml methanol). The disk was sealed with a two-layered foil as described previously (Steigert et al. 2007). In brief, a composite foil consisting of a 500  $\mu\text{m}$  high melting foil with thin 2–5  $\mu\text{m}$  low melting layer is bonded to the microfluidic disk at 120°C. The high melting foil has a glass transition temperature of  $\sim 130^\circ\text{C}$  (TOPAS 6013) and the low melting layer of  $\sim 75^\circ\text{C}$  (TOPAS 8007). This allows the thin binding layer to melt at the bonding temperature while the substrate and sealing foil remain intact.

### 3 Results and discussion

Three alternative variants of the aliquoting structure were characterized in terms of metering precision. The alter-

pneumatic valve releases the metered volumes into the receiving chambers. The two-stage principle provides fluidic separation of the receiving chambers by the air gaps of the metering channels and feed channel as well as especially via the tiny channels of the centrifuge-pneumatic valves.

#### 3.1 Measurement of liquid volumes

The liquid volumes in the receiving chambers were determined by stroboscopic camera pictures taken under rotation. The relevant measured variable is the filling level of the chamber  $h$ , defined as the lowest point of the liquid meniscus. For these measurements, all receiving chambers were formed roughly rectangular. In Fig. 4, the geometry parameters relevant for volume determination are depicted. The liquid volume  $V$  in the receiving chamber can then be approximated as

$$V = V(h, w, d, V_{\text{lid}}, V_{\text{meniscus}}) = h \cdot w \cdot d + V_{\text{lid}} + V_{\text{meniscus}}, \quad (1)$$

where  $h$  is the measured filling level,  $w$  and  $d$  are the width and depth of the chamber,  $V_{\text{lid}}$  is the additional volume due to the flexible lid that expands under rotation, and  $V_{\text{meniscus}}$  is the volume difference from a cuboid due to the surface tension leading to a curved meniscus.

In an ideally manufactured structure,  $V = V(h)$ , since all other values are constant. In a real structure,  $V$  can still be derived linearly from  $h$ , but with the uncertainty  $\Delta V$  (propagation of error):

$$\Delta V = \sqrt{\left(\frac{\partial V}{\partial h} \Delta h\right)^2 + \left(\frac{\partial V}{\partial w} \Delta w\right)^2 + \left(\frac{\partial V}{\partial d} \Delta d\right)^2 + \left(\frac{\partial V}{\partial V_{\text{lid}}} \Delta V_{\text{lid}}\right)^2 + \left(\frac{\partial V}{\partial V_{\text{meniscus}}} \Delta V_{\text{meniscus}}\right)^2}, \quad (2)$$

native variants were produced by micro-milling, thermoforming of foils, or injection molding, in order to demonstrate the versatility of the design. The following rotational frequency protocol was used for microfluidic operation of the structure: in a first operation phase at low rotational frequencies ( $\sim 10$  Hz), the liquid proceeds through a sloping feed channel, filling branching metering channels (Fig. 3). The liquid in the metering channels stops at the centrifuge-pneumatic valve. Continuing rotation, excess liquid overflows through the feed channel into the waste, thus defining metered volumes. The second phase is introduced by elevating the rotational frequency to about 25 Hz. At this frequency, the centrifuge-

where  $\Delta h$  is the observational error of the filling level (assumed as 2 pixels in a camera image),  $\Delta w$  and  $\Delta d$  the production tolerance in width and depth, respectively,  $\Delta V_{\text{lid}}$  the variance among different chambers due to lid expansion, and  $\Delta V_{\text{meniscus}}$  the variance among chambers due to the meniscus. Since  $\Delta V_{\text{lid}}$  and  $\Delta V_{\text{meniscus}}$  only depend on material constants which are the same for all chambers (elasticity of lid, surface tension of liquid, and contact angle...), they are assumed to be negligible.

Since volume-dependent tests can be calibrated with samples of known composition, the volume precision is more crucial for reliable test results than volume accuracy. Due to the unknown variables  $V_{\text{lid}}$  and  $V_{\text{meniscus}}$ , the

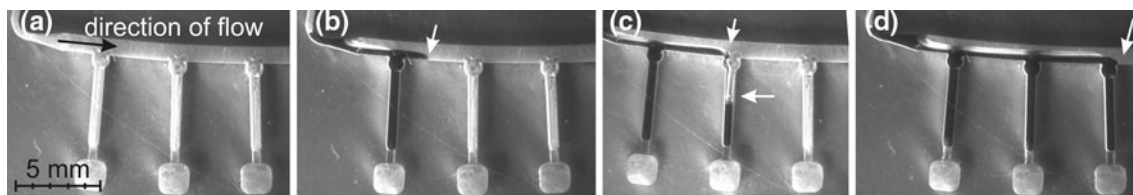


**Fig. 3** Illustration of the liquid distribution process. **a–d** Time progresses from the *left image* to the *right*. The *white arrows* indicate the position of the liquid meniscus. The centrifugo-pneumatic valve is

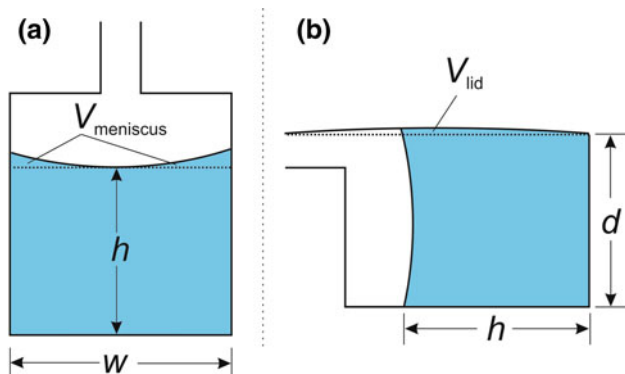


**Fig. 4** Sketch of observable liquid level in a single receiving chamber and relevant geometry parameters. **a** *Top view* the liquid fills the chamber with a width  $w$  up to a height  $h$ , which is defined as the lowest point of the meniscus. The liquid volume outside  $h$  has the volume  $V_{meniscus}$ . **b** *Side view* the chamber has the depth  $d$ . Since the chamber is observed from the bottom, the visible filling level  $h$  is the foremost point of the meniscus. Due to the flexibility of the lid, an additional volume  $V_{lid}$  has to be considered under rotation

volume accuracy of the aliquoting structure is difficult to determine precisely. However, the volume precision can be approximated by the sample standard deviation  $s$  for  $N$  samples. The following relation exists between the volume standard deviation  $s(V)$  and the filling level standard deviation  $s(h)$ :

$$s(V) = \sqrt{\frac{1}{(N-1)} \sum_{i=1}^N (V_i(h) - \bar{V})^2}$$

$$= wd \sqrt{\frac{1}{(N-1)} \sum_{i=1}^N (h_i - \bar{h})^2} = wd \cdot s(h), \tag{3}$$

with  $\bar{V}$  and  $\bar{h}$  being the mean volume and mean height of the liquid in the chamber, respectively. Therefore, the coefficient of variation (CV) for the volume is:

$$CV = \frac{s(V)}{\bar{V}} = \frac{wd \cdot s(h)}{wd \cdot \bar{h} + V_{lid} + V_{meniscus}}$$

$$= \frac{s(h)}{\bar{h} + (V_{lid} + V_{meniscus})/(wd)} := \frac{s(h)}{\bar{h} + \alpha} \tag{4}$$

with the correction term  $\alpha$  defined as written in Eq. 4. The correction term contains the volume corrections due to lid

designed to hold at the metering frequency. Thus, no liquid enters the receiving chambers during the metering process

expansion and liquid meniscus, which are estimated from visual inspection of the lid expansion under pressure and the area of the liquid meniscus under rotation. Both values are comparably small, since the lid lift off is estimated to be 20  $\mu\text{m}$  at 1.2 bar by visual inspection and the meniscus volume under rotation is estimated to be in the order of magnitude of 0.2  $\text{mm}^3$ .

### 3.2 Micro-milled structure

First, a micro-milled prototype of the aliquoting structure was tested. To evaluate the precision of the fluidic metering structure, a design with elongated receiving chambers was used, allowing a more precise measurement of final filling levels (Fig. 5a). Samples with 105  $\mu\text{l}$  were filled into the inlet chamber and aliquoted by a two-stage centrifugation with 10 and 28 Hz into 16 aliquots of 6  $\mu\text{l}$  each plus waste. The final liquid levels in the receiving chambers were measured as captured by a camera. The first and last receiving chamber showed significantly higher and lower filling levels (up to 20%), respectively, and were not included in the evaluation. The reason for this is that the first metering channel burst first and collected some residual fluid from the feed channel. The lower filling level in the last metering channel is attributed to creeping of liquid into the waste chamber during the metering stage. The problem with the higher filling level in the first chamber was solved later by increasing the centrifugation frequency from 10 Hz (metering) to 28 Hz (forwarding) gradually in 1.7 Hz steps every second. This led to an almost complete drain of the feed channel into the waste before the burst frequency was reached. The problem with the lower liquid volume in the last chamber was rectified by replacing the waste by a sacrificial metering structure with downstream centrifugo-pneumatic valve and receiving chamber (Fig. 6b). The mean filling level of the remaining receiving chambers was 2.8 mm with  $\alpha = 0.06$  mm resulting in a CV of the metered volumes of 2.8% according to Eq. 4 (Fig. 5b). The production tolerance of the milled structure was determined with a contactless optical profilometer (TESA VISIO 300 DCC, TESA Switzerland SA, Switzerland). Typical measured tolerances

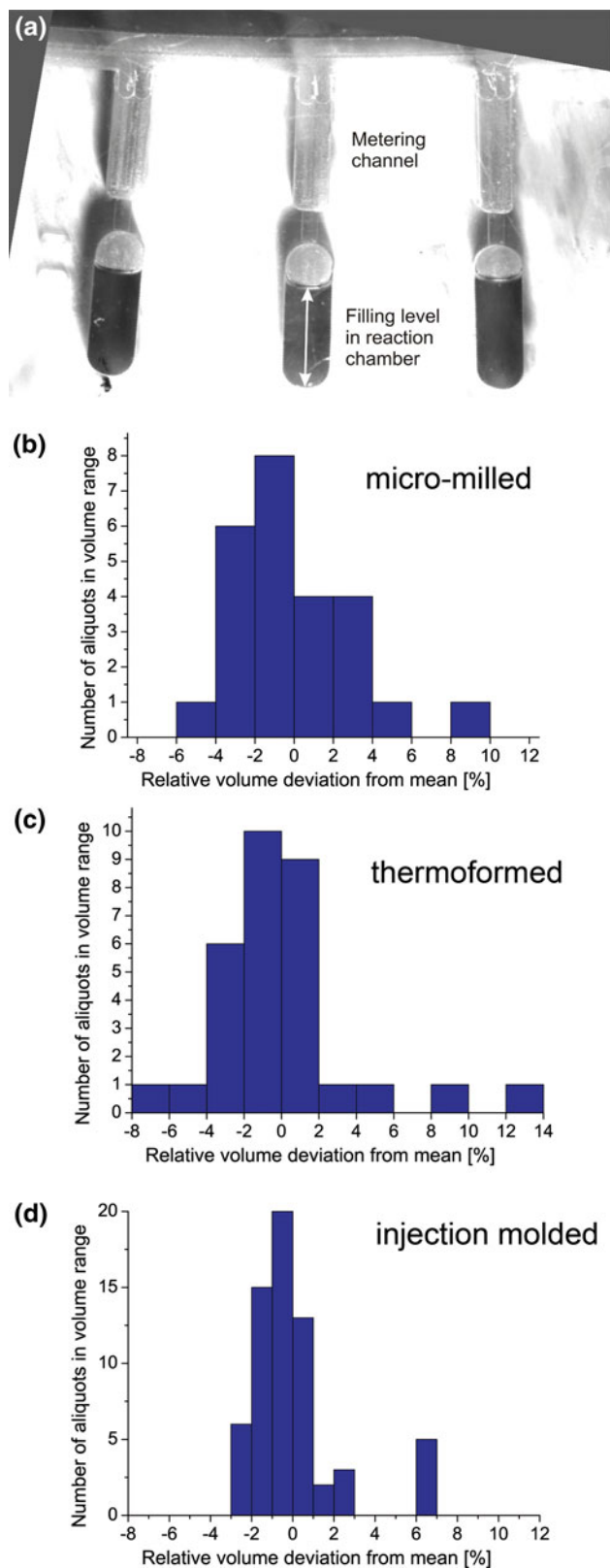


**Fig. 5** Metering precision of the aliquoting structure. **a** Measurement of the filling levels in elongated receiving chambers at a rotational frequency of 28 Hz. The filling height  $h$  was obtained by measuring the distance between the bottom of the receiving chamber and the lowest point of the air–liquid interface in the captured image. **b** Histogram of metering precision for the milled structure, first and last chamber not included. **c** Histogram of the metering precision in a thermoformed foil with a redesigned transition to the waste chamber (see Fig. 6a). All chambers are included. **d** Histogram of metering precision for the injection-molded structure (see Fig. 6b). The metering precision is significantly improved due to the precise production technology

were in the order of 20  $\mu\text{m}$ . For determining the error in the filling level  $h$ , a measurement error of 2 pixels of the camera image of the filling levels was assumed (one at the upper and one at the lower end of the liquid column). This corresponds to a measurement error of 30  $\mu\text{m}$ . Considering the production tolerances  $\Delta w = \Delta d = 20 \mu\text{m}$  and an observational error of  $\Delta h = 30 \mu\text{m}$ , the total uncertainty according to Eq. 2 equals  $\Delta V \approx 0.15 \mu\text{l}$  which corresponds to 2.5% of the target filling volume 6  $\mu\text{l}$ . The variations of the measured volume and the measurement uncertainty are very close to each other, demonstrating the high precision of the aliquoting structure.

### 3.3 Thermoformed foil

In order to test the performance of the aliquoting structure with different manufacturing processes amenable to mass production, two additional designs were fabricated by thermoforming and injection molding. The layout for foil thermoforming was designed to split a 90- $\mu\text{l}$  volume into 8 aliquots of 10  $\mu\text{l}$  each plus waste (Fig. 6a). In order to adapt the design to the different demands of the production process, sharp corners were rounded for foil thermoforming which did not prevent a precise metering. With an  $\alpha$  value of 0.03 mm, the volume CV of the metering process was 3.6%, as can be seen in the histogram for the foil design (Fig. 5c, first and last chamber included). The production tolerances of the thermoformed foil are essentially governed by the tolerances of the milled master (Focke et al. 2010), so they are again assumed to be 20  $\mu\text{m}$ . Considering a production tolerance of  $\Delta w = \Delta d = 20 \mu\text{m}$  and an observational error of  $\Delta h = 30 \mu\text{m}$ , the total uncertainty is  $\Delta V \approx 0.21 \mu\text{l}$  which corresponds to 2.1% of the target filling volume 10  $\mu\text{l}$ . Compared to the uncertainty  $\Delta V$ , the higher CV could indicate an additional disturbance, possibly an incomplete drain of the feed channel into the waste which could be corrected by a higher feed channel slope.

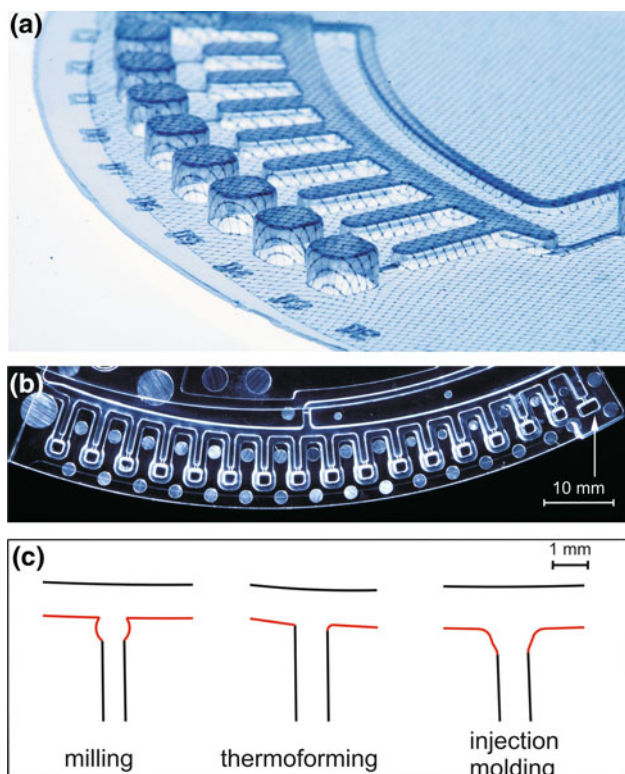


**Fig. 6** Aliquoting structure for alternative production technologies. **a** Aliquoting structure in thermoformed foil with printed grid. The unstretched grid has a 500  $\mu\text{m}$  edge length. **b** Aliquoting structure in injection-molded cartridge. The arrow highlights the modified waste structure. **c** Transitions from feed channel to metering channel in designs for milling, thermoforming, and injection molding. Besides other small variations in channel diameters and slope, the sharp corners at the transition from feed channel to metering channel are smoothed out for thermoforming and injection-molded designs to account for design rules at these replication technologies. The structure is functional for all shown alternatives

One issue with processing the aliquoting structure on the foil disk was the maximum rotational frequency of 27 Hz achievable with this particular processing instrument (Focke et al. 2010). At this frequency, a complete drain of the metering channels into the receiving chamber was not always achieved for centrifugo-pneumatic valves with burst frequencies  $>12$  Hz. It was observed that the forwarding of the liquid into the receiving chamber could stop prematurely. In order to overcome this limitation, a different operation mode for the aliquoting structure was established by simulation and experiment. This so-called unidirectional shake-mode operation relies on frequency changes between a high (e.g. 25 Hz) and low (e.g. 6 Hz) frequency in order to subsequently empty the metering channel. This operation mode always led to a complete forwarding of the liquid into the receiving chamber. A detailed description is given in Sect. 4.

### 3.4 Injection-molded structure

The design was also validated on injection-molded polymer disposables (microfluidic ChipShop GmbH, Germany). The injection-molded design splits a 100  $\mu\text{l}$  liquid volume into 16 sub-volumes of 6  $\mu\text{l}$  plus waste (Fig. 6b). Due to the very high precision of injection-molded test disks, the CV of the sub-volumes improved significantly to 2.2% over all chambers (Fig. 5d) with a correction term  $\alpha = 0.03$  mm. The lateral tolerances of the injection-molded structures were again measured with the TESA VISIO 300 DCC and were determined to be in the order of 5  $\mu\text{m}$ . The depth could not be measured accurately, since the very smooth surface could not be recognized easily by the optical measurement system. Since the depth of the receiving chamber is larger

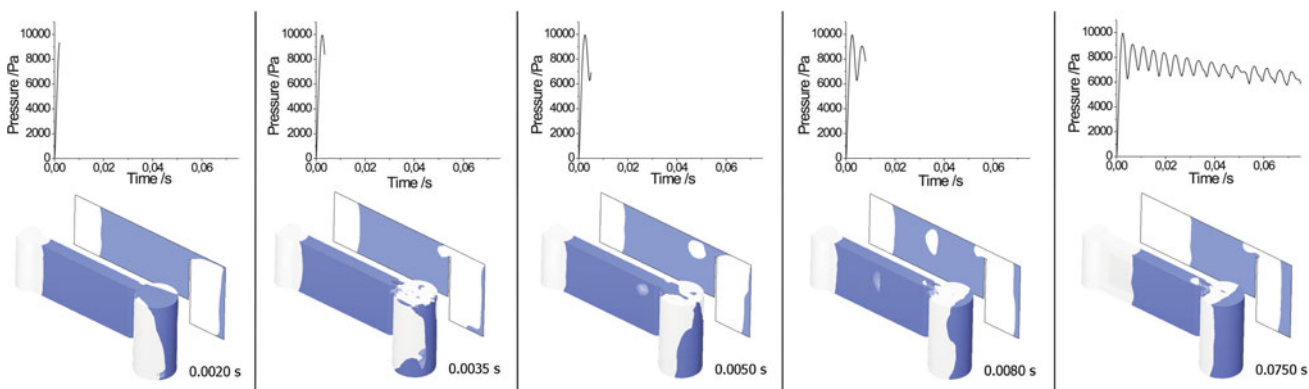


**Fig. 7** CFD simulation of a valve burst at 24 Hz. The graphs in the upper part show the pressure above ambient pressure in the circular receiving chamber, the lower part shows a 3D view and a cut along the center of the channel. At 2 ms, the pressure in the receiving chamber builds up to about 10 kPa. Between 3.5 and 5 ms, a part of

the entrapped air is released as a bubble along the metering channel and the pressure decreases. At 8 ms, another bubble is forming after a second buildup in pressure. At the end of the simulation at 75 ms, a total of 15 bubbles have formed and the chamber is filled to about 1/3

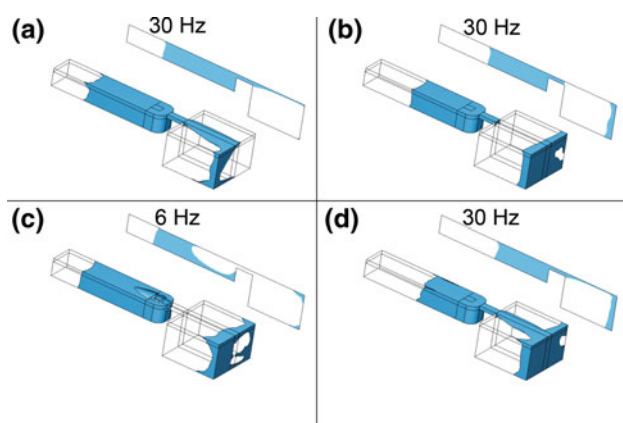


**Fig. 8** CFD simulation of the “unidirectional shake-mode” operation. For this simulation, the receiving chamber has been modeled as a cuboid for a shorter calculation time. **a–b** The valve is operated at a rotational frequency of 30 Hz. Due to the compression of air in the receiving chamber, this leads to a stop of the filling process after some time. **c** A reduction of the rotational frequency to 6 Hz allows the air in the receiving chamber to expand and some of the air is vented along the metering channel. **d** A consecutive increase in rotational frequency to 30 Hz allows the transport of further liquid into the receiving chamber

than the width but should be governed by similar relative errors, it was estimated to be in the range of 10  $\mu\text{m}$ . Considering the production tolerance  $\Delta w = 5 \mu\text{m}$ ,  $\Delta d = 10 \mu\text{m}$  and an observational error of  $\Delta h = 30 \mu\text{m}$ , the total volume uncertainty is  $\Delta V \approx 0.14 \mu\text{l}$  which corresponds to 2.3% of the target filling volume 6  $\mu\text{l}$ . In the current design, the last two receiving chambers consistently contained a higher liquid volume. If the last two chambers are not included in the statistics, the CV is reduced to 1.1%. A possible improvement could include a redesign of the transition region to the waste chamber with a higher radial slope. For the injection-molded structure, the CV drops below the measurement uncertainty. This is possible, since statistically,  $\sim 32\%$  of the values in a normally distributed measurement series are found outside one standard deviation from the mean value, whereas the measurement uncertainty gives the theoretical maximum deviation from the true value.

It can be concluded from the experimental characterization that the promoted aliquoting structure is compatible with the commonly used prototyping and fabrication technologies such as milling, injection molding, and foil thermoforming. It is also tolerant against the slight changes in geometry that needed to be implemented for being compatible with the design rules of the different fabrication methods (Fig. 6c), without loss of precision. This demonstrates the robustness of the structure and its suitability for mass production. Especially, the injection-molded design shows the potential for highly precise aliquoting with CVs in the range of 1–2%.

## 4 Simulations

The metering and forwarding phases as the basic building blocks of the aliquoting structure run on the sub-second timescale and are difficult to observe under rotation. For a better understanding of the filling process, we performed a numerical simulation using a computational fluid dynamics software (CFD-ACE+ from ESI-Group, ESI-Group 2007) and compared the results to our experimental findings. The simulations focused on the burst mechanism of the centrifugo-pneumatic valve, the unidirectional shake-mode operation, and the influence of the centrifugo-pneumatic valve on the precision of the aliquoting.

### 4.1 Burst mechanism

In a first step, forwarding of liquid from the metering structure through the valve into the receiving chamber was simulated. Figure 7 shows a typical simulated image series of a bursting centrifugo-pneumatic valve during the first 75 ms. It clearly shows partial venting of the receiving chamber at high centrifugal frequencies via air bubbles rising through the metering channel, as described previously (Mark et al. 2009). These results show that the valving process is composed of intermittent exchange of liquid and air along the narrow connection channel. As described in Sect. 2, this exchange can sometimes stall at lower centrifugal frequencies. In the following simulations, it was analyzed, if this process can be restarted. Additionally, it is investigated, whether air–liquid exchange already occurs in the metering stage, leading to metering errors.

### 4.2 Unidirectional shake-mode operation

One investigated approach to restart a stalled liquid–air exchange was to alternate between a high and a low rotational frequency (Fig. 8). This operation mode was labeled “unidirectional shake-mode”. At low frequencies (e.g. 6 Hz), this leads to a reduced centrifugal pressure which permits the expansion of the compressed air in the receiving chamber into the metering channel, where part of it rises as bubbles. The now decreased air pressure permits further flow into the receiving chamber at higher frequencies (e.g. 25 Hz). This unidirectional shake-mode operation was successfully implemented to ensure complete forwarding of liquids into the receiving chambers, especially on processing instruments with maximum rotational frequencies below 30 Hz.

### 4.3 Influence of the centrifugo-pneumatic valve on the metering accuracy

We also theoretically investigated the systematic metering error of the centrifugo-pneumatic valve due to a potential

release of a small amount of liquid into the receiving cavity before the stabilizing pressure of the valve is built up. This parameter is important to control since it could represent a systematic metering error and potentially start reactions in the receiving chamber prematurely, if they are triggered by liquid (e.g. dissolving of lyophilized reagents). To get an idea of the maximum volume entering the receiving chamber during the metering process, we simulated a water plug of 4.63 mm length (6  $\mu\text{l}$ ) at a metering frequency of 9 Hz. The volume of liquid intruding into the receiving chamber before forming a stable liquid–air interface at that frequency was 0.12  $\mu\text{l}$  for a 400  $\mu\text{m}$  connection channel depth and less for smaller geometries. This systematic error amounts to 2% or less of the total volume of 6  $\mu\text{l}$ . In order to reduce this effect, smaller connection channel geometries should be preferred.

## 5 Conclusions

The presented aliquoting method enables an easy way to integrate aliquoting steps for assay automation in centrifugally driven lab-on-a-chip systems at the downstream end of the assay. The aliquoting structure is robust even in the presence of detergents or ethanol as shown previously (Mark et al. 2009). With the unidirectional shake-mode, a low frequency operation mode of the aliquoting structure was investigated and confirmed by CFD simulation. The two step metering approach provides fluidic separation between the aliquots which prevents cross-contamination between chambers. The metered volume is defined solely by the geometry of the metering structures and is, therefore, independent of the volume of pre-stored reagents in the receiving chambers. A potential application of such a structure is to perform panel tests, such as homogeneous immunoassays, clinical chemistry tests, or molecular diagnostic tests for genotyping or pathogen detection, from one sample. The structure does not require any local or global surface modifications and proved to be compatible with the commonly used prototyping and fabrication processes—micro-milling, injection molding, and thermoforming—demonstrating robustness, ease of implementation, and potential for mass production.

**Acknowledgments** The authors gratefully acknowledge financial support by the German Federal Ministry of Education and Research (project Zentrilab, grant No. 16SV2347). Part of this work was funded by the Federal Ministry of Education and Research (BMBF) under the Research Programme for Civil Security of the German Federal Government as part of the High-Tech Strategy for Germany (project SONDE, grant No. 3N10116). The authors also gratefully acknowledge financial support by the European Union (project MagRSA, contract No. 037957).

## References

- Andersson P, Ekstrand G (2007) Retaining microfluidic microcavity and other microfluidic structures. (US7300199)
- Burtis CA, Anderson NG, Mailen JC, Scott CD, Tiffany TO, Johnson WF (1972) Development of a miniature fast analyzer. *Clin Chem* 18(8):753–761
- Cho YK, Lee JG, Park JM, Lee BS, Lee Y (2008) Lab-on-a-disc for simultaneous analysis of blood chemistry and immunoassay. In: Proceedings of 12th international conference on miniaturized systems for chemistry and life sciences ( $\mu\text{TAS}$ )
- Ducree J, Haeberle S, Lutz S, Pausch S, von Stetten F, Zengerle R (2007) The centrifugal microfluidic bio-disk platform. *J Micro-mech Microeng* 17(7):103–115
- ESI-Group (2007) CFD-ACE+ 2007. <http://www.esi-group.com/>
- Focke M, Stumpf F, Faltin B, Reith P, Bamarni D, Wadle S, Müller C, Reinecke H, Schrenzel J, Francois P, Mark D, Roth G, Zengerle R, von Stetten F (2010) Microstructuring of polymer films for highly sensitive genotyping by real-time PCR on a centrifugal microfluidic platform. *Lab Chip* 10(19):2519–2526. doi:10.1039/C004954A
- Gorkin R, Park J, Siegrist J, Amasia M, Lee BS, Park JM, Kim J, Kim H, Madou M, Cho YK (2010) Centrifugal microfluidics for biomedical applications. *Lab Chip* 10(14):1758–1773
- Haeberle S, Zengerle R (2007) Microfluidic platforms for lab-on-a-chip applications. *Lab Chip* 7(9):1094–1110. doi:10.1039/b706364b
- Honda N, Lindberg U, Andersson P, Hoffman S, Takei H (2005) Simultaneous multiple immunoassays in a compact disc-shaped microfluidic device based on centrifugal force. *Clin Chem* 51(10):1955–1961
- Liu RH, Yang JN, Lenigk R, Bonanno J, Grodzinski P (2004) Self-contained, fully integrated biochip for sample preparation, polymerase chain reaction amplification, and DNA microarray detection. *Anal Chem* 76(7):1824–1831
- Lutz S, Weber P, Focke M, Faltin B, Hoffmann J, Müller C, Mark D, Roth G, Munday P, Armes NA, Piepenburg O, Zengerle R, von Stetten F (2009) Microfluidic lab-on-a-foil for nucleic acid analysis based on isothermal recombinase polymerase amplification of DNA. *Lab Chip* 10:887–893. doi:10.1039/B921140C
- Madou M, Zoval J, Jia GY, Kido H, Kim J, Kim N (2006) Lab on a CD. *Annu Rev Biomed Eng* 8:601–628
- Mark D, Metz T, Haeberle S, Lutz S, Ducrée J, Zengerle R, von Stetten F (2009) Centrifugo-pneumatic valve for metering of highly wetting liquids on centrifugal microfluidic platforms. *Lab Chip* 9:3599–3603. doi:10.1039/B914415C
- Mark D, Haeberle S, Roth G, von Stetten F, Zengerle R (2010) Microfluidic lab-on-a-chip platforms: requirements, characteristics and applications. *Chem Soc Rev* 39:1153–1182. doi:10.1039/B820557B
- Nolte DD (2009) Invited review article: review of centrifugal microfluidic and bio-optical disks. *Rev Sci Instrum* 80(10):101101–101122
- Rubenstein KE, Schneider RS, Ullman EF (1972) “Homogeneous” enzyme immunoassay. A new immunochemical technique. *Biochem Biophys Res Commun* 47(4):846–851. doi:10.1016/0006-291X(72)90570-0
- Schembri CT, Ostoich V, Lingane PJ, Burd TL, Buhl SN (1992) Portable simultaneous multiple analyte whole-blood analyzer for point-of-care testing. *Clin Chem* 38(9):1665–1670
- Schembri CT, Burd TL, Kopfsill AR, Shea LR, Braynin B (1995) Centrifugation and capillarity integrated into a multiple analyte whole-blood analyzer. *J Autom Chem* 17(3):99–104
- Sharp DH (1984) An overview of Rayleigh–Taylor instability. *Physica D* 12:3–18

- Siegrist J, Gorkin R, Bastien M, Stewart G, Peytavi R, Kido H, Bergeron M, Madou M (2010) Validation of a centrifugal microfluidic sample lysis and homogenization platform for nucleic acid extraction with clinical samples. *Lab Chip* 10(3):363–371
- Steigert J, Haeberle S, Brenner T, Muller C, Steinert CP, Koltay P, Gottschlich N, Reinecke H, Ruhe J, Zengerle R, Dürée J (2007) Rapid prototyping of microfluidic chips in COC. *J Micromech Microeng* 17(2):333–341
- Sundberg SO, Wittwer CT, Gao C, Gale BK (2010) Spinning disk platform for microfluidic digital polymerase chain reaction. *Anal Chem* 82(4):1546–1550